Theory for charge and orbital density-wave states in manganite $La_{0.5}Sr_{1.5}MnO_4$

Zi-Jian Yao[1], Wei-Qiang Chen[2,1], Jin-Hua Gao[3,1], Hong-Min Jiang[1,4], Fu-Chun Zhang[1]
[1] *Department of Physics and Center of Theoretical and Computational Physics, The University of Hong Kong, Hong Kong, China*
[2] *Department of Physics, South University of Science and Technology of China, Shenzhen, China*
[3] *Department of Physics, Huazhong University of Science and Technology, Wuhan, 430074, China*
[4] *Department of Physics, Hangzhou Normal University, Hangzhou, China*

(Dated: today)

We propose that the high temperature disordered phase in manganites may be described by spinless e_g electrons. The interactions of spinless electrons may lead to charge and orbital ordered states. Our theory explains the Fermi surface probed in angle resolved photoemission spectroscope and the observed simultaneous phase transition to charge and orbital ordered state in $La_{0.5}Sr_{1.5}MnO_4$. The orbital orderings are shown to be $d_{x^2-y^2} \pm d_{3z^2-r^2}$.

PACS numbers:

Introduction. The manganese oxides are prototype materials for the rich physics of the interplay among spin, charge and orbital degrees of freedom, which has been an important issue in correlated electron systems [1–5]. Because of the strong electron-electron interactions, standard perturbation theories are not appropriate to study these systems. It has been a challenge to develop proper theoretical methods to study the phenomena.

In this paper, we consider single-layered perovskite $La_{0.5}Sr_{1.5}MnO_4$, which shows orbital and charge orderings, followed by spin long range order, as temperature T decreases. We propose that the basic physics of the high temperature phase and its phase transition may be understood in the large Hund's coupling limit, where the electronic structure is described by two-fold Mn-3d e_g-orbital electrons, whose spins are confined to be parallel to the local t_{2g} electrons. At the high temperature, the local spins are random, and the electronic structure is described by the two e_g spinless fermions. The transition to the charge and orbital ordered states is driven by the interactions between these spinless fermions, and can be examined by using mean field approximations. Our theory predicts a Fermi surface (FS) with a volume as twice as large of that of the spin-1/2 fermions, consistent with the recent angle resolved photoemission spectroscope (ARPES) and explains the simultaneous orbital and charge orderings in the single layered $La_{0.5}Sr_{1.5}MnO_4$. The theory is also consistent with the experiments of the bi-layered $La_{1.2}Sr_{1.8}Mn_{1.2}O_7$ [6] and $La_{1.2}Sr_{1.8}Mn_{1.2}O_7$ [7].

Manganese $La_{0.5}Sr_{1.5}MnO_4$ exhibits two phase transitions. The high temperature phase transition occurs at $T = T_{co} \approx 220$ K, at which the system becomes charge and orbital ordered [8, 9]. The charge density has a checkerboard distribution, and the orbital has an ordered wave vector $(\pi/2, \pi/2)$. The low temperature phase transition occurs at $T = T_N \approx 110$ K, at which the antiferromagnetic spin ordering emerges [10]. The low temperature phase transition has been studied previously [11], here we shall focus on the high temperature phase and the related phase transition.

In $La_{0.5}Sr_{1.5}MnO_4$, the manganese atoms are arranged into a two-dimensional square lattice. Each manganese atom is surrounded by six oxygen atoms. The electrons are well confined in the plane so that this compound is a quasi two-dimensional material. The crystal field splits the energy levels into a high energy e_g orbitals ($d_{x^2-y^2}$ and $d_{3z^2-r^2}$), and a lower energy t_{2g} orbitals (d_{xy}, d_{yz}, and d_{zx}). There are 3.5 d-electrons per Mn atom, which suggests 0.5 electron distributed in the two e_g orbitals whose spin is confined with a local spin-3/2 of the t_{2g} electrons due to the strong Hund's coupling.

$La_{1-x}Sr_{1+x}MnO_4$ is insulating for all Sr concentrations x. However, the remnant FS, which is about 190 meV below the chemical potential, has been probed by ARPES [12]. The observed fermiology consists of a large hole-like FS around (π, π) and a very small electron pocket around $(0, 0)$. The segment of the hole-like FS is quite flat, which may induce good FS nesting and lead to charge and orbital orderings [12].

In the large Hund's coupling limit, the spin of the e_g electron is parallel to the local spins and the charge configuration on each Mn site i takes the values $n_{i,\alpha} = 0, 1$, with $n = c^\dagger_{i\alpha} c_{i\alpha}$, and $\alpha = 1, 2$ labeling orbitals $d_{x^2-y^2}$ and $d_{3z^2-r^2}$, respectively. The interaction part of the Hamiltonian, including the the Coulomb interactions U_0 (on-site) and V (nearest neighbor, NN), is given by (see supplement material for a detailed derivation),

$$H_I = U_0 \sum_i n_{i1} n_{i2} + \frac{V}{2} \sum_{\langle ij \rangle} (n_{i1} + n_{i2})(n_{j1} + n_{j2}), \quad (1)$$

where the sum of i runs over all the sites on a square

lattice, $\langle ij\rangle$ represents NN pairs. Note that the spin polarization of the e_g electrons is implied.

The kinetic energy term of the e_g electrons can be described by an NN hopping matrix of the two e_g-orbitals. The single particle part of the Hamiltonian reads,

$$H_0 = -\sum_{\langle ij\rangle,\alpha,\beta} t^{\alpha,\beta}_{i\sigma_i,j\sigma_j} c^\dagger_{i\alpha\sigma_i} c_{j\beta\sigma_j} + H.c. \qquad (2)$$

σ_i is the spin orientation of the t_{2g} electrons at site i. The hopping integrals between the two sites depend on the relative spin orientation of the two spins. In the semi-classical limit, we have $t^{\alpha,\beta}_{i\sigma_i,j\sigma_j} = \cos(\frac{\theta_{ij}}{2}) t^{\alpha,\beta}_{ij}$ with θ_{ij} the relative angle of the two spins at sites i and j.

The solution of H_0 strongly depends on the spin configurations of the localized t_{2g} electrons. Here we consider a high temperature phase where the spins are random, and approximate $\cos(\frac{\theta_{ij}}{2}) \approx \langle\cos(\frac{\theta}{2})\rangle$, which is an averaged value of the solid angle and is independent of the pair $\langle ij\rangle$. Then we have $t^{\alpha\beta}_{i\sigma_i,j\sigma_j} = \langle\cos(\frac{\theta}{2})\rangle t^{\alpha\beta}_{ij}$, and H_0 is reduced to a usual tight-binding model for spinless fermions. The pre-factor $\langle\cos(\frac{\theta}{2})\rangle$ represents a reduction of the hopping integral due to the random spins. Note that the average value of $\cos(\frac{\theta}{2})$ in the solid angle space is $1/3$. H_0 then can be written as,

$$H_0 = -\langle\cos(\frac{\theta}{2})\rangle \sum_{\vec{k}\alpha\beta} 2t^{\alpha\beta}\gamma_{\alpha\beta}(\vec{k}) c^\dagger_{\vec{k}\alpha} c_{\vec{k}\beta}, \qquad (3)$$

where $t^{\alpha\beta}$ is the hopping integral along the x-axis. $\gamma_{11} = \gamma_{22} = \gamma_+$, $\gamma_{12} = \gamma_{21} = \gamma_-$, and $\gamma_\pm(\vec{k}) = \cos k_x \pm \cos k_y$. In what follows, we shall study $H = H_0 + H_I$ by solving H_0 first and studying the effect of H_I in Eq. (2) from a weak coupling approach.

H_0 can be diagonalized and the eigen-energy is given by

$$\epsilon_\pm = -\langle\cos\theta/2\rangle(t^{11}+t^{22})\gamma_+(\vec{k}) \pm \sqrt{(t^{11}-t^{22})^2\gamma_+(\vec{k})^2 + 4(t^{12})^2\gamma_-^2}.$$

The hopping matrix elements are related by Slater-Koster formalism [13] if we consider the direct hopping between the two NN Mn sites, from which we obtain $t^{22} = t^{11}/3$ and $t^{12} = t^{21} = -t^{11}/\sqrt{3}$. Hereafter, we will take $\langle\cos\theta/2\rangle t^{11}$ as the energy unit.

Fig. 1(a) shows the calculated FS for the quarter filling of e_g electrons, namely 0.5 electron per Mn-site, relevant to the single layer $La_{0.5}Sr_{1.5}MnO_4$. The area inside the FS is one half of the Brillouin zone (BZ), consistent with the Luttinger sum rule for the spinless fermions. The shape of the FS is in good agreement with the ARPES data, which we reproduce here at the upper-right of 1/4 of the BZ. Note that the small Fermi pocket probed in the ARPES centered at Γ point may be reproduced in our theory by slightly increasing the number of carriers. As we can see, a large segment of the FS is quite flat, and there is a clear nesting at the wave vector $\vec{q} = (\pi/2, \pi/2)$, which suggests possible instabilities toward ordered states.

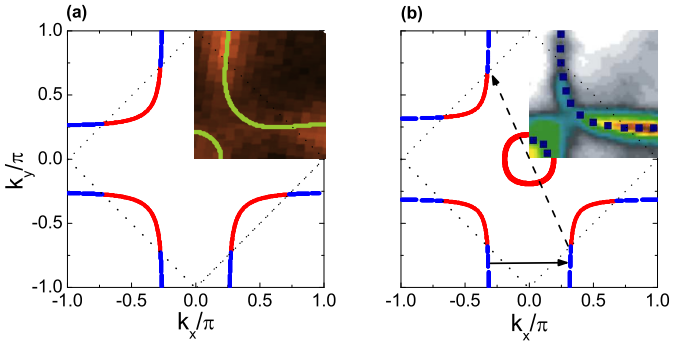

FIG. 1: FS of the spinless fermion model H_0. (a) is for e_g electron density n=0.5 per site, and (b) is for n=0.6. Red and blue colors on the Fermi sheets represent the states mostly orbital $d_{x^2-y^2}$ or $d_{3z^2-r^2}$, respectively. The upper-right $\frac{1}{4}$ BZ in (a) and (b) show the FS observed in the ARPES experiments on single layered $La_{0.5}Sr_{1.5}MnO_4$ [12] and on bi-layered $La_{1.2}Sr_{1.8}Mn_{1.2}O_7$ [14], respectively. The colors used in ARPES data represent intensity, while the blue dots in (b) are added here to guide the eyes.

Fig. 1(b) shows the FS for electron number 0.6 per Mn site, corresponding to the electron density of the bi-layer compound $La_{1.2}Sr_{1.8}Mn_{1.2}O_7$ [6], where the electron layer splitting can be neglected. The shape of the Fermi surface is in good agreement with the ARPES result of the bi-layered compound, with a Fermi area of 60% of the BZ, and the nesting wave vectors $\vec{q}_1 = (0.6\pi, 0)$ and $\vec{q}_2 = (0.6\pi, 0.6\pi)$. This is again in support of the spinless fermion scenario.

Orbital density wave instability. We now study the effect of H_I. We will first identify the most plausible instabilities by using the random phase approximation (RPA) analysis. We then apply a mean field approach to examine the phase transitions. To study the density-wave instabilities, we define the following orbital (o) and charge (c) density operators,

$$\rho^o_i = n_{i+} - n_{i-} = c^\dagger_{i1}c_{i2} + c^\dagger_{i2}c_{i1},$$
$$\rho^c_i = n_{i+} + n_{i-} = c^\dagger_{i1}c_{i1} + c^\dagger_{i2}c_{i2}, \qquad (4)$$

where the orbitals + and − are linear combinations of the orbitals $d_{x^2-y^2}$ and $d_{3z^2-r^2}$,

$$c^\dagger_{i\pm} = \frac{1}{\sqrt{2}}(c^\dagger_{i1} \pm c^\dagger_{i2}). \qquad (5)$$

As it will become clear later, the orbital ordering in this problem is associated with orbitals + and −, instead of 1 and 2. We introduce a static susceptibility matrix χ, whose element is defined as

$$\chi_{\alpha\alpha',\mu'\mu}(q) = \frac{1}{2}\int_0^\beta d\tau \,\langle T_\tau \rho_{\alpha\alpha'}(\vec{q},\tau)\rho_{\mu\mu'}(-\vec{q},0)\rangle\,. \qquad (6)$$

where $\rho_{\alpha\alpha'}(\vec{q}) = \sum_{\vec{k}} c^\dagger_{\vec{k}+\vec{q},\alpha} c_{\vec{k}\alpha'}$

The orbital and charge susceptibilities are then given by

$$\begin{aligned}\chi^c(\vec{q}) &= \tfrac{1}{2}\textstyle\sum_{\alpha\mu}\chi_{\alpha\alpha,\mu\mu}(\vec{q}),\\ \chi^o(\vec{q}) &= \tfrac{1}{2}\textstyle\sum_{\alpha\mu}\chi_{\alpha\bar{\alpha},\mu\bar{\mu}}(\vec{q}).\end{aligned} \tag{7}$$

Within the RPA, we have

$$\hat{\chi} = (\hat{I} + \hat{\chi}^{(0)}\hat{U}^c)^{-1}\hat{\chi}^{(0)}. \tag{8}$$

In the above equation, $\hat{I}$ is an identity operator, and $\hat{\chi}^{(0)}$ is the matrix of the bare susceptibility,

$$\chi^{(0)}_{\alpha\beta,\mu\nu}(\vec{q}) = \frac{1}{N}\sum_{\vec{k}mn} a^{\alpha*}_m(\vec{k}+\vec{q})a^\beta_n(\vec{k})a^{\nu*}_n(\vec{k})a^\mu_m(\vec{k}+\vec{q})$$
$$\times[f(\epsilon_n(\vec{k}+\vec{q})) - f(\epsilon_m(\vec{k}))]/[\epsilon_m(\vec{k}) - \epsilon_n(\vec{k}+\vec{q}) + i\eta], \tag{9}$$

where m and n are the band indices, and $a^\alpha_m(\vec{k}) = \left\langle \alpha, \vec{k}|m, \vec{k}\right\rangle$ is the orbital weight. We arrange the matrix index from 1 to 4 as $(\alpha\beta) = (11)$, (22), (12), and (21). The interaction matrix $\hat{U}^c$ is of the form $\hat{U}^c = \hat{U}^1 \oplus \hat{U}^2$, where $\hat{U}^1 = V(\vec{q})\sigma_0 + (V(\vec{q}) + U_0)\sigma_1$, and $\hat{U}^2 = -U_0\sigma_0$ with σ_0 an identity matrix and σ_1 the first Pauli matrix.

In the matrix representation described above, the upper-left 2 by 2 block in χ describes charge part and the lower-right block describes the orbital part, as we can see from Eqs. (7). While $\hat{U}^c$ is block diagonal, $\chi^{(0)}(\vec{q})$ is generally not block diagonal, so that the charge and orbital are coupled in the response functions. A special case is at $q_x = \pm q_y$, where the off-diagonal components of $\hat{\chi}$ vanishes due to the symmetry in the band structure [15]. This property makes the study of the instability at $\vec{q} = (\pi/2, \pi/2)$ and $\vec{q} = (\pi, \pi)$ simpler. We will show that in this case, the inter-orbital nesting connecting the different segments of the FS between orbital 1 and orbital 2 favors the $\pm$ orbital ordering. To illustrate this point, we define orbitals $c^\dagger_\alpha = \cos(\psi)c^\dagger_1 + \sin(\psi)c^\dagger_2$ and $c^\dagger_\beta = \sin(\psi)c^\dagger_1 - \cos(\psi)c^\dagger_2$, with orbital density $\rho^o_\psi = c^\dagger_\alpha c_\alpha - c^\dagger_\beta c_\beta$. Note that in the vicinity of orbital-density-wave instability, the nesting is between electron states with mainly orbitals 1 and mainly orbital 2, we have

$$\chi^o_\psi \approx \cos(\psi)\sin(\psi)\sum_{\alpha\mu}\chi_{\alpha\bar{\alpha},\mu\bar{\mu}}, \tag{10}$$

which reaches its maximum with $\psi = \pi/4$. Therefore we conclude that the ordered orbitals are $+$ and $-$ (for a more detailed discussion, see [16]).

We have found three types of instabilities in our calculations, namely the orbital ordering at $(\pi/2, \pi/2)$ and at $(\pi/2, 0)$, and the charge ordering at (π, π). Note that the orbital orderings are related to the FS nesting, while the charge ordering is not. In Fig. 2 we plot the susceptibilities at corresponding wave vectors as functions of interaction strengths. As we can see, the orbital susceptibilities at $(\pi/2, \pi/2)$ and $(\pi/2, 0)$ are greatly enhanced

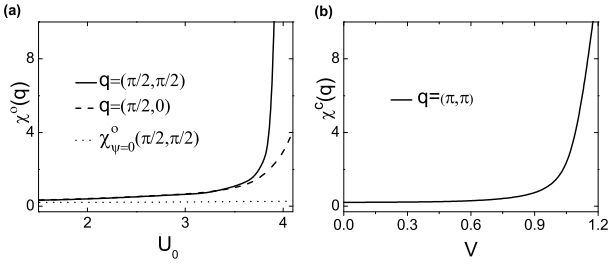

FIG. 2: $T = 0$ RPA susceptibilities. (a): Orbital susceptibility $\chi^o(\vec{q})$ at $\vec{q} = (\pi/2, \pi/2)$ and $(\pi/2, 0)$ for orbital ordering between $+$ and $-$. The dotted line is the susceptibility for orbital ordering between orbitals 1 and 2. $V = 0$. (b): Charge susceptibility $\chi^c(\vec{q})$ at $\vec{q} = (\pi, \pi)$ with $U_0 = 0$.

by the inter-orbital repulsion U_0, and the susceptibility at $(\pi/2, \pi/2)$ is much larger at large U_0 with a critical value of $U_0 \approx 4$ for the ordering. Note that the orbital susceptibility based on the ordering between orbitals $d_{x^2-y^2}$ and $d_{3z^2-r^2}$, $\chi^o_{\psi=0}(\pi/2, \pi/2)$, is much weaker as we can see from the dotted line in Fig. 2(a). For the charge ordering at (π, π), as seen in Fig. 2(b), χ^c diverges at $V \approx 1.1$, which indicates a phase transition to (π, π) charge ordering.

Phase diagram and phase transition. The RPA calculations above have indicated two possible major instabilities, the $(\pi/2, \pi/2)$ orbital order (OO) and (π, π) charge order (CO). Below we use mean field approach to examine the interplay between the two orderings. We introduce the two mean fields

$$\begin{aligned}\langle\rho^o_i\rangle &= \left\langle c^\dagger_{i1}c_{i2} + c^\dagger_{i2}c_{i1}\right\rangle = \rho_o\cos(\mathbf{q}_1\cdot\mathbf{r}_i + \phi),\\ \langle\rho^c_i\rangle &= \left\langle c^\dagger_{i1}c_{i1} + c^\dagger_{i2}c_{i2}\right\rangle = \rho_c\cos(\mathbf{q}_2\cdot\mathbf{r}_i) + \bar{\rho},\end{aligned} \tag{11}$$

with $\mathbf{q}_1 = (\pi/2, \pi/2)$, $\mathbf{q}_2 = (\pi, \pi)$, and $\bar{\rho} = 0.5$. ρ_o and ρ_c are the order parameters of charge and orbital, respectively, while ϕ is the phase shift in the real space of the orbital order. The mean field Hamiltonian then reads

$$\begin{aligned}H_{\rm MF} = H_0 &- \frac{U_0}{4}\sum_{\mathbf{k}}\left[\rho_o e^{i\phi}(c^\dagger_{\mathbf{k},2}c_{\mathbf{k}+\mathbf{q}_1,1} + c^\dagger_{\mathbf{k},1}c_{\mathbf{k}+\mathbf{q}_1,2}) + H.c.\right]\\ &- 4(V - U_0/8)\rho_c\sum_{\mathbf{k}\alpha}c^\dagger_{\mathbf{k}\alpha}c_{\mathbf{k}+\mathbf{q}_2\alpha},\end{aligned} \tag{12}$$

The self consistent equations for the mean fields are

$$\begin{aligned}\rho_o e^{i\phi} &= \frac{2}{N}\sum_{\mathbf{k}}\left\langle c^\dagger_{\mathbf{k}+\mathbf{q}_1,1}c_{\mathbf{k},2} + c^\dagger_{\mathbf{k}+\mathbf{q}_1,2}c_{\mathbf{k},1}\right\rangle\\ \rho_c &= \frac{1}{N}\sum_{\mathbf{k}\alpha}\left\langle c_{\mathbf{k}+\mathbf{q}_2,\alpha}c_{\mathbf{k},\alpha}\right\rangle.\end{aligned} \tag{13}$$

By solving $H_{\rm MF}$ together with the self-consistent equations (13), we obtain the zero temperature phase diagram, which is shown in fig. 3. In the calculation, we found only two possible phase shift ϕ for the orbital

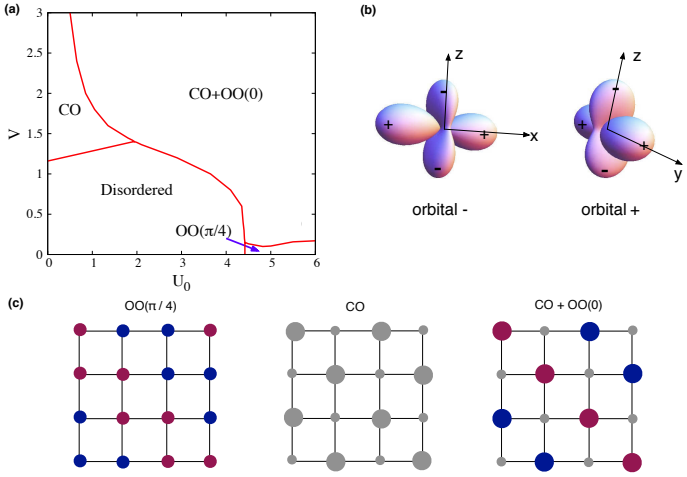

FIG. 3: (a). Phase diagram of spinless fermion model at zero temperature. CO: charge-ordered phase; OO: orbital-ordered phase. (b) Shapes of ordered orbitals + and −. (c) Illustration of the ordered states in real space. Electron charge is represented by the size of the circle. Orbitals are represented by colors: Blue for dominant orbital +, maroon for dominant orbital -, and grey for orbital-disordered site.

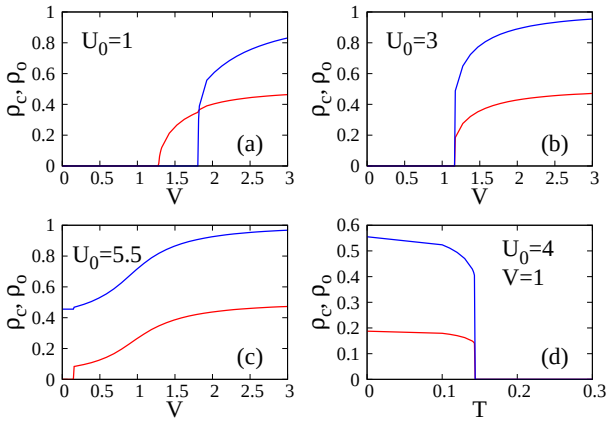

FIG. 4: Panels (a), (b), and (c): V dependence of orbital ordering ρ_o (blue curves) and charge ordering ρ_c (red curves) at $U_0 = 1$. (a) at $U_0 = 0$; (b) at $U_0 = 3$; (c) at $U_0 = 5.5$. Panel (d): Temperature dependence of orbital ordering ρ_o (blue curves) and charge ordering ρ_c (red curves) at $U_0 = 4, V = 0.5$.

ordering, $\phi = \pi/4$ and $\phi = 0$, which are denoted as OO($\pi/4$) and OO(0), respectively, in the phase diagram. The real space modulation of each phase is sketched in Fig. 3(c). One of the main features of the phase diagram is that the system is in the coexistence phase of CO and OO(0) in a large parameter space of (U_0, V). The phase with only orbital ordered only appears in a tiny phase space with very small V and large U_0. We also note that there is a sudden change on the orbital ordering phase from OO($\pi/4$) in the absence of CO to OO(0) in the presence of CO. Below we shall provide some understanding of the later. Let us first consider the orbital ordered only phase. The preferred phase OO($\pi/4$) may be understood as the result of losing less kinetic energy due to the orbital ordering. The amplitude of the orbital order parameter $\langle \rho_i^o \rangle$ for the OO($\pi/4$) phase is $\rho_o/\sqrt{2}$, while the amplitude for the OO(0) phase is ρ_o. However, the situation is very different in the presence of charge ordering. In that case, the local orbital order $\langle \rho_i^o \rangle$ is bound by the local charge density of electrons $\langle \rho_i \rangle$. Because $\langle \rho_i \rangle$ are reduced on some sites, the charge ordering suppresses the OO($\pi/4$) phase. On the other hand, the OO(0) is consistent with and may even be enhanced by the charge ordering. In the limit of strong charge ordering $\rho_c = 1/4$, the kinetic energy term diminishes, and $\langle \rho_o \rangle = 1$ in the phase OO(0), in comparison with a maximum value of $\langle \rho_o \rangle = 0.5$ in the absence of charge ordering. In other words, the presence of charge order will induce the OO($\pi/4$) phase. The transition from OO($\pi/4$) phase to CO+OO(0) phase is the first order.

In Fig. 4(a)-(c), we plot the orbital and charge order parameters as functions of V for various U_0 at T=0. At small $U_0 = 1$, as V increases, CO develops first followed by a coexistent phase with the OO(0) order. At $U_0 = 3$, the transition to the charge and orbital ordered state is simultaneous as V increases, and is first order with clear jumps in the order parameters. At large $U_0 = 5.5$, we have only orbital ordering at small V, and co-existent phase with charge ordering. And at the charge ordering point, the orbital order parameter has a change in both the phase (not shown here but discussed before) and its magnitude. In Fig. 4(d), we show the order parameters as functions of temperature for $(U_0 = 4, V = 1)$, to illustrate the simultaneous first order phase transition of the orbital and charge orderings at finite temperature, which may explain the simultaneous orderings observed in experiment of $La_{0.5}Sr_{1.5}MnO_4$ [9]. Note that the mean field theory predicts a large first order transition, which may change the electronic structure dramatically under the transition. Since mean field theories usually over-estimate the order parameter jumps in the first order phase transition, the interpretation of this should be more cautious.

We now discuss the ordered orbital characters of the system. Different from the usual rotational invariant spin-1/2 space, the kinetic energy term is not symmetric with respect to the rotation in the pseudo-spin e_g orbital space. Therefore, there is a selection of specific orbitals for the orbital-density wave ordering. In the early theories the ordered orbitals have been predicted to be $d_{3x^2-z^2}$ and $d_{3y^2-z^2}$ [17]. However, in more recent x-ray analysis [18], it is found that the ordering of $d_{x^2-z^2}$ and $d_{y^2-z^2}$ is much more compatible with linear dichroism measurements. Note that the two orbitals $d_{x^2-z^2}$ and $d_{y^2-z^2}$ are not orthogonal. To further examine this issue, we have performed the mean field calculations to examine the ordering between a general linear combination of d_{3z^2} and $d_{x^2-y^2}$, and have found that the ordering between + and − has the lowest energy. Therefore,

in contrast to previous arguments that the ordered orbitals are non-orthogonal, we propose that at temperature $T_N \leq T \leq T_{co}$, the ordered orbitals are orthogonal orbitals + and −, which are essentially equal mixtures of $d_{3z^2-r^2}$ and $d_{x^2-y^2}$. The shape of each orbital is plotted in Fig. 3(b).

In summary, we have studied the high temperature states and the high temperature phase transition in single layered manganite $La_{0.5}Sr_{1.5}MnO_4$. We propose that the basic physics of the high temperature states in this class of strongly correlated systems may be described by an effective spinless Hamiltonian with two e_g electrons. The FS calculated within the model in the absence of the remaining interaction is in good agreement with the ARPES data. The orbital and charge density wave orderings may be studied based on the model with the remaining Coulomb interactions. Our mean field theory predicts a simultaneous charge and orbital orderings in a large parameter space, consistent with the experiments in $La_{0.5}Sr_{1.5}MnO_4$. The ordered orbital characters are predicted to be a linear combination of $d_{x^2-y^2}$ and $d_{3z^2-r^2}$ with the equal amplitudes, which may be further justified in experiments. The effective Hamiltonian may be applied to other systems of strong correlations.

Supplementary material: effective spinless model for manganites with strong Hund's rule coupling

We consider a model Hamiltonian $H = H_0 + H_I$, with H_0 the single particle part to describe conduction e_g electrons and H_I the interaction part to describe the Coulomb repulsion between two e_g electrons and an on-site spin coupling of an e_g electron and spin-$\frac{3}{2}$ of the localized t_{2g} electrons. We first consider the interaction Hamiltonian, which is given by

$$\begin{aligned}\mathcal{H}_I =& U\sum_{i\alpha} n_{i\alpha\uparrow}n_{i\alpha\downarrow} + (U' - \frac{1}{2}J)\sum_i n_{i1}n_{i2} \\ & - 2J\sum_i \vec{s}_{i1}\cdot\vec{s}_{i2} + J\sum_i c^\dagger_{i1\uparrow}c^\dagger_{i1\downarrow}c_{i2\downarrow}c_{i2\uparrow} \\ & - J\sum_{i\alpha}\vec{s}_{i\alpha}\cdot\vec{S}_i + \frac{V}{2}\sum_{<i,j>}(n_{i1}+n_{i2})(n_{j1}+n_{j2}),\end{aligned} \tag{14}$$

where U, U' are on-site intra- and inter- orbital direct Coulomb repulsive interactions, respectively, and $J > 0$ the exchange Coulomb interaction or the Hund's rule coupling. By symmetry, $U = U' + 2J$. V is the nearest neighbor (n.n.) site Coulomb interaction. $\vec{s}_{i\alpha}$ is the spin of an electron of orbital α at site i. We denote $\alpha = 1$ for $d_{x^2-y^2}$ orbital and $\alpha = 2$ for $d_{3r^2-z^2}$ orbital. $\vec{S}_i$ is the spin-$\frac{3}{2}$ of three localized t_{2g} electrons at site i, and $n_{i\alpha} = n_{i\alpha\uparrow} + n_{i\alpha\downarrow}$ is the total electron number operator for a given orbital. In our model, the inter-orbital Coulomb repulsion between e_g and t_{2g} electrons is a constant, which can be absorbed into the chemical potential.

We consider the large Hund's coupling limit, where U, U', J are much larger than the kinetic energy term H_0 below. We shall assume, however, $U' - J$ to be comparable with the kinetic energy, and may even be treated as a perturbation from a technical point of view. We may argue for this limit that in a metallic phase, the Coulomb interaction U' has a good screening, while the Hund's coupling J is not screened, so that $U' - J$ could be small. We will further discuss this point in the summary of the paper. In this limit, $\vec{s}_{i\alpha}$ is parallel to $\vec{S}_i$, and doubly occupied e_g electrons on the same site is allowed because it costs an energy of $U' - J$. Since the local spin degrees of freedom of e_g electrons are frozen, the e_g electrons behave like spinless fermions. We remark that this scenario is consistent with the recent ARPES measurements. The average number of e_g electrons in the single layer compound $La_{0.5}Sr_{1.5}MnO_4$ is 0.5 per Mn-site by valence counting. The Fermi volume measured in the ARPES is expected to be 25% of the area of the first Brillouin zone for spinful fermions and 50% of the zone area for spinless fermions according to the Luttinger sum rule. The ARPES data for the single-layered manganites [12] shows that the area enclosed by the Fermi surface (Fermi lines in 2D) is about 49% of the zone area, in excellent agreement with the spinless fermion scenario, but not spinful fermion scenario. Similarly, the ARPES data for the bilayer compound $La_{1.2}Sr_{1.8}Mn_{1.2}O_7$ give us an estimate of the area enclosed by the Fermi surface to be about 60% of the Brillouin zone, consistent with the spinless fermion scenario for this compound where the average number of e_g electron is 0.6 per Mn site [6, 14]. Note that the spin degrees of freedom of the e_g electron is frozen only locally, and the spins at different Mn sites, hence the spins of e_g electrons at different sites, may have different polarizations. H_I in the large Hund's coupling limit then takes the form,

$$H_I = U_0\sum_i n_{i1}n_{i2} + \frac{V}{2}\sum_{<i,j>}(n_{i1}+n_{i2})(n_{j1}+n_{j2}), \tag{15}$$

with $U_0 = U' - J$, and the spin polarization of the e_g electrons is implied.

[1] Y. Tokura and N. Nagaosa, Science **288**, 462 (2000).

[2] E. Dagotto, T. Hotta, and A. Moreo, Physics Reports **344**, 1 (2001), ISSN 0370-1573.

[3] E. Dagotto, New Journal of Physics **7**, 67 (2005).

[4] J. van den Brink, G. Khaliullin, and D. Khomskii, Phys. Rev. Lett. **83**, 5118 (1999).

[5] D. V. Efremov, J. van den Brink, and D. I. Khomskii, Nature Materials **3**, 853 (2004).

[6] Y.-D. Chuang, A. D. Gromko, D. S. Dessau, T. Kimura, and Y. Tokura, Science **292**, 1509 (2001).

[7] J. Trinckauf, T. Hänke, V. Zabolotnyy, T. Ritschel, M. O. Apostu, R. Suryanarayanan, A. Revcolevschi, K. Koepernik, T. K. Kim, M. von Zimmermann, et al., Physical Review Letters **108**, 16403 (2012).

[8] Y. Moritomo, Y. Tomioka, A. Asamitsu, Y. Tokura, and Y. Matsui, Phys. Rev. B **51**, 3297 (1995).

[9] Y. Murakami, H. Kawada, H. Kawata, M. Tanaka, T. Arima, Y. Moritomo, and Y. Tokura, Physical Review Letters **80**, 1932 (1998).

[10] E. O. Wollan and W. C. Koehler, Phys. Rev. **100**, 545 (1955).

[11] M. Daghofer, A. M. Oles, D. R. Neuber, and W. von der Linden, Physical Review B **73**, 104451 (2006).

[12] D. V. Evtushinsky, D. S. Inosov, G. Urbanik, V. B. Zabolotnyy, R. Schuster, P. Sass, T. Hänke, C. Hess, B. Büchner, R. Follath, et al., Physical Review Letters **105**, 147201 (2010).

[13] J. C. Slater and G. F. Koster, Physical Review **94**, 1498 (1954).

[14] N. Mannella, W. L. Yang, X. J. Zhou, H. Zheng, J. F. Mitchell, J. Zaanen, T. P. Devereaux, N. Nagaosa, Z. Hussain, and Z.-X. Shen, Nature **438**, 474 (2005).

[15] The block off-diagonal index can generally be written to be $(\alpha, \alpha, \alpha, \bar{\alpha})$ and its cyclic. Under the exchange of k_x and k_y, we have dispersion $\epsilon_\pm(k_x, k_y) = \epsilon_\pm(k_y, k_x)$, and the orbital weight $a_n^\alpha(k_x, k_y)a_n^{\beta*}(k_x, k_y) = (-1)^{\alpha+\beta}a_n^\alpha(k_y, k_x)a_n^{\beta*}(k_y, k_x)$. Therefore at $q_x = q_y$, we have $\chi^0_{\alpha\alpha,\alpha\bar{\alpha}}(q_x, q_y) = -\chi^0_{\alpha\alpha,\alpha\bar{\alpha}}(q_y, q_x) = 0$. The same analysis can be applied to show the other block off-diagonal elements vanish at $\vec{q} = (q_x, \pm q_x)$.

[16] Z.-J. Yao, J.-X. Li, Q. Han, and Z. D. Wang, Europhysics Letters **93**, 37009 (2011).

[17] J. B. Goodenough, Phys. Rev. **100**, 564 (1955).

[18] D. J. Huang, W. B. Wu, G. Y. Guo, H.-J. Lin, T. Y. Hou, C. F. Chang, C.-T. Chen, A. Fujimori, T. Kimura, H. B. Huang, et al., arXiv **92**, 87202 (2004).